UC Davis
Mechanical and Aerospace Engineering

Title
Molecular dynamics study of the thermal properties and phenomena of graphane and fluorographene

Permalink
https://escholarship.org/uc/item/0pn70122

Author
Chen, Junjie

Publication Date
2024-06-10

Supplemental Material
https://escholarship.org/uc/item/0pn70122#supplemental

eScholarship.org Powered by the California Digital Library
University of California

Molecular dynamics study of the thermal properties and phenomena of graphane and fluorographene

Junjie Chen [a, b, *]

[a] Department of Mechanical and Aerospace Engineering, College of Engineering, University of California, Davis, California, 95616, United States

[b] Department of Energy and Power Engineering, School of Mechanical and Power Engineering, Henan Polytechnic University, Jiaozuo, Henan, 454000, P.R. China

* Corresponding author, E-mail address: junjiem@tom.com

Abstract

In spite of significant efforts to investigate the ability of hydrogenated and fluorinated graphene to conduct heat, little research has focused particularly upon their other thermal properties, such as thermal contraction and heat capacity, which have implications for the development of thermal nanotechnology. In an attempt to determine these thermal properties, a few experiments have been carried out, with rather conflicting results. In the present study, calculations were performed using molecular dynamics to investigate the thermal properties of graphane and fluorographene and especially the phenomena involved. The thermal expansion coefficients and heat capacities of the two-dimensional materials were determined at different temperatures. The results indicated that graphane is thermally contracted more significantly than graphene. The calculated molar heat capacity at constant volume is about 25.00 J/(mol·K) for graphene and about 29.26 J/(mol·K) for graphane. The specific heat capacity of fluorographene is always lower than that of graphane. A negative relationship does exist between the binding energy and the temperature.

Keywords: Thermal properties; Carbon materials; Molecular dynamics; Structural configurations; Material properties; Thermal phenomena

1. Introduction

Graphene is an atomically thick, two-dimensional sheet made up of densely packed carbon atoms in a hexagonal shape. Graphene can be regarded as a parent form of all the other graphitic carbon allotropes. Graphite is a three-dimensional crystal consisting of relatively weakly coupled graphene layers. Carbon nanotubes may be represented as scrolls of graphene. Buckyballs are spherical molecules made from graphene with some hexagonal rings replaced by pentagonal rings. Peculiar properties and the unique two-dimensional structure endow graphene with unique natures, for example, the fractional quantum Hall effect [1, 2], ballistic transport of charge carriers [3], and an ambipolar electric field effect [4]. Modern electronics are basically two-dimensional in that they use mainly the surface of semiconducting materials. Therefore, graphene and other two-dimensional materials are considered very promising for many such applications. Unfortunately, graphene may be undesired or disadvantageous for practical electronic applications. Graphene as a two-dimensional material is electrically conducting, which makes it difficult to directly manufacture transistors. Transistors are the active components of integrated circuits, in which a semiconductor material with tunable band gaps is required. Hydrogenation, which is a reaction of great industrial importance [5, 6], will lead to structural transformation of the valence orbitals of carbon atoms, for example, formation of sp^3 hybrid orbitals from sp^2 hybrid orbitals. This may open an energy gap in the gapless electronic spectrum of graphene by creating positive holes in the conducting π-band [7, 8]. Significantly, the energy gap can be tuned to

the desired conductivity, depending crucially upon the ordering and distribution of hydrogen atoms and the ratio of the number of carbon atoms to the number of hydrogen atoms [9, 10]. Consequently, hydrogenated graphene has especially great potential for practical electronic applications.

Graphane is a two-dimensional, honeycomb hydrogenated form of graphene, and its properties and structure can be manipulated by reversible hydrogenation [11, 12]. Graphane was predicted theoretically a decade and a half ago [8], which is the fully hydrogenated analogue of graphene. For this new two-dimensional material, the electronic properties change markedly [13, 14], since hydrogenation interrupts the π-bonding system of graphene while retaining the original hexagonal bonding arrangement [15, 16]. Accordingly, graphene, which is highly conductive, is converted from a semimetal into an insulator. This two-dimensional material may therefore have more favourable electronic properties than graphene for certain applications [17, 18]. Furthermore, the structure and conductivity of graphene may be fully restored, since hydrogenation is reversible. This reversibility gives rise to possible high efficiency hydrogen storage. Two favourable distinguishable conformations of graphane exist, designated as chair and boat. The chair conformation of graphane has a staggered arrangement of all its carbon-hydrogen bonds. The boat conformation lacks perfect staggering of bonds, with hydrogen atoms alternating in pairs. Various chemical routes for synthesizing graphane have been determined [8], such as the Birch reduction of graphite, and the substitution reaction of fluorinated graphene by replacing fluorine atoms with hydrogen atoms with suitable reagents. Initially, graphane sheets were isolated experimentally by hydrogenation of graphene [19]. A variety of other methods have then been suggested [20]. The size of the graphane sheets produced varies from nanometres across to millimetres, depending upon the desired morphology.

Halogenated graphene, also referred to as graphene halide, can have similar structure and attributes as graphane. Fluorographene is a fluorocarbon derivative of graphene. As a typical example of halogenated graphene, fluorographene can be synthesised by exposing surfaces of suspended graphene to an environment containing atomic fluorine. There are extensive efforts underway to investigate the properties of fluorographene for numerous applications [21, 22]. Fluorographene inherits the mechanical strength of graphene, with high thermal and chemical stability [23, 24]. Fluorographene can be strongly insulating or semiconducting. Suitable electronic properties can be introduced into fluorographene through chemistry technology so as to use in semiconductor devices. For example, the spin-splitting and band gap can be tailored by changing the concentration of fluorine [25]. Stable semiconducting fluorographene can expand the range of possibilities offered by graphene, thereby allowing it to be modified chemically to satisfy specific requirements in practical applications [26], for example, electronics and related optoelectronics fields. Fluorographene can be derived by chemical modification of graphene [27] or by exfoliation from multilayer crystals, for example, graphite fluoride [28]. However, incomplete or partial fluorination may cause instability and the loss of atomic fluorine [29, 30], thereby rendering fluorographene problematic to accomplish the fluorination reaction to any significant degree. Furthermore, partially fluorinated graphene conducts current to a lesser extent at room temperature and does not have a well-defined energy gap.

In spite of significant efforts to investigate the structural and electronic properties of hydrogenated and fluorinated graphene, little research has focused particularly on their thermal properties and the phenomena involved. In practice, most research is focused upon unlocking and tuning the band gaps necessary to create heterojunction bipolar transistors by hydrogenation or fluorination of graphene. While the thermal properties of hydrogenated and fluorinated graphene have attracted increasing attention, the research efforts have so far focused upon their thermal conductivities. In particular, progress has been made towards determining the melting point and thermal stability of these two-dimensional materials [31, 32]. However, little research has been conducted to determine their other thermal properties and phenomena, such as thermal contraction and heat capacity. A clear

understanding of the thermal problems involved is needed, which may provide a basis for further research on other material properties. For example, the mechanisms of the thermal rippling and stability of these crystals are crucial for understanding their electronic transport processes [33, 34]. The inability of conducting spatially resolved measurements underscores the need for atomistic and molecular modelling. In the present study, molecular dynamics simulations were performed to investigate the thermal properties of graphane and fluorographene and especially the phenomena involved, including the thermal expansion coefficients and heat capacities at different temperatures. Additionally, the structural configurations were determined by performing first-principles calculations. Furthermore, comparisons of thermal properties and the phenomena involved were made computationally between pristine and functionalised graphene. The present study aims to provide a clear understanding of the thermal problems involved in hydrogenated and fluorinated graphene. Particular emphasis is placed on the thermal contraction and heat capacity of these materials.

2. Computational methods

Calculations are performed using molecular dynamics to investigate the thermal properties of graphane and fluorographene and especially the phenomena involved in the thermodynamic process when subjected to changes in temperature. Thermal expansion is the general increase in the volume of a material as its temperature is increased. It is usually expressed as a fractional change in length or volume per unit temperature change. A linear expansion coefficient is usually employed in describing the expansion of a solid, while a volume expansion coefficient is more useful for a liquid or a gas. If a crystalline solid is isometric, the expansion will be uniform in all dimensions of the crystal. If it is not isometric, there may be different expansion coefficients for different crystallographic directions, and the crystal will change shape as the temperature changes. In a solid or liquid, there is a dynamic balance between the cohesive forces holding the atoms or molecules together and the conditions created by temperature. Higher temperatures imply greater distance between atoms. Different materials have different bonding forces and therefore different expansion coefficients.

Atomic interactions are modelled using the second-generation reactive empirical bond order potential for hydrocarbons, for example, graphane employed in the present study, in the situations in which accurate but efficient descriptions of chemical reactivity are required [35, 36]. The chemical binding energy E_b for short-range interactions is determined as follows:

$$E_b = \sum_i \sum_{j(>i)} \left(V^R\left(r_{ij}\right) - b_{ij} V^A\left(r_{ij}\right) \right), \tag{1}$$

wherein b_{ij} connotes the many-body, bond-order term, r_{ij} is the scalar distance between atoms i and j, the attraction term, V^A, captures the atomic attraction because of valence electrons forming covalent bonds, and the repulsive pair term, V^R, refer to a representative of the Pauli repulsion between electron clouds. The formalism of the attraction and repulsive pair terms is given by

$$V^A\left(r_{ij}\right) = f_C\left(r_{ij}\right) \sum_{n=1,2,3} B_n e^{\left(-\beta_n r_{ij}\right)}, \tag{2}$$

$$V^R\left(r_{ij}\right) = f_C\left(r_{ij}\right)\left(1 - \frac{Q}{r_{ij}}\right) A e^{\left(-\alpha r_{ij}\right)}, \tag{3}$$

in which α, A, β_n, B_n, and Q are the pair parameters depending upon the type of chemical bonding.

The bond order term encompasses all the multibody effects to modulate the covalent bonding between atoms [37, 38]:

$$b_{ij} = \frac{1}{2}\left(b_{ij}^{\sigma\text{-}\pi} + b_{ji}^{\sigma\text{-}\pi}\right) + b_{ij}^{DH} + \Pi^{RC}, \tag{4}$$

where the first two terms capture the dependence of bond energy upon bond angle and coordination, and the last two terms capture the dependence of bond energy upon torsion and conjugation, respectively. The term $b_{ij}^{\sigma\text{-}\pi}$ can be written as follows:

$$b_{ij}^{\sigma\text{-}\pi} = \left(1 + \sum_{k \neq i,j} f_C\left(r_{ij}\right) G\left(\cos\left(\theta_{jik}\right)\right) e^{\left(\lambda_{jik}\left(r_{ij} - R_{ij}^{e}\right) - \left(r_{ik} - R_{ik}^{e}\right)\right)} + P_{ij}\left(N_i^C, N_i^H\right)\right)^{-\frac{1}{2}}, \tag{5}$$

wherein k denotes a nearest neighbour of atom i, excluding atom j, and G and P are angle and coordination functions, respectively.

The conjugation term Π^{RC} is a tri-cubic spline function

$$\Pi^{RC} = F_{ij}\left(N_i^t, N_j^t, N_{ij}^{conj}\right), \tag{6}$$

where N_i^t and N_j^t denote the total number of neighbours of atoms i and j, respectively, and N_{ij}^{conj} denotes the number of conjugate neighbours. This term captures the dependence of bond energy upon conjugation [37, 38]. The number of conjugate neighbours depends upon the number of carbon neighbours of atoms i and j

$$N_{ij}^{conj} = 1 + \left(\sum_{k \neq i,j}^{carbon} f_C\left(r_{ik}\right) F\left(x_{ik}\right)\right)^2 + \left(\sum_{l \neq i,j}^{carbon} f_C\left(r_{jl}\right) F\left(x_{jl}\right)\right)^2, \tag{7}$$

$$x_{ik} = N_i^t - f_C\left(r_{ik}\right), \tag{8}$$

$$F\left(x_{ik}\right) = 1, \; x_{ik} < 2, \tag{9}$$

$$F\left(x_{ik}\right) = \frac{1}{2}\left(1 + \cos\left(2\pi\left(x_{ik} - 2\right)\right)\right), \; 2 < x_{ik} < 3, \tag{10}$$

$$F\left(x_{ik}\right) = 0, \; x_{ik} > 3. \tag{11}$$

A dihedral function is utilised to capture the rotation of groups around a carbon-carbon bond

$$b_{ij}^{DH} = T_{ij}\left(N_i^t, N_j^t, N_{ij}^{conj}\right)\left(\sum_{k \neq i,j}^{carbon} \sum_{l \neq i,j}^{carbon} \left(1 - \cos^2 \Theta_{kijl}\right) f_C\left(r_{jl}\right) f_C\left(r_{ik}\right)\right), \tag{12}$$

in which T_{ij} is a tri-cubic spline function, f_C is the cutoff function, and Θ_{kijl} is the torsional angle between atoms k, i, j, and l. The function $\cos\Theta_{kijl}$ is determined as follows:

$$\cos\Theta_{kijl} = \left(\vec{r}_{ik} \cdot \vec{r}_{ij}\right) \cdot \left(\vec{r}_{ij} \cdot \vec{r}_{jl}\right) \cdot \left(r_{ik} r_{jl} r_{ij}^2 \sin\theta_{jik} \sin\theta_{ijl}\right)^{-1}. \tag{13}$$

Long-range atomic interactions are modelled using the Lennard-Jones potential. A bicubic spline function is used to interpolated smoothly the Lennard-Jones potential with the second-generation reactive empirical bond order potential

$$V_{ij}^{LJ} = 4\varepsilon_{ij}\left(\left(\frac{\sigma_{ij}}{r_{ij}}\right)^{12} + \left(\frac{\sigma_{ij}}{r_{ij}}\right)^{6}\right). \tag{14}$$

Mixing rules are used to calculate the parameters σ_{ij} and ε_{ij}

$$\sigma_{ij} = \frac{1}{2}\left(\sigma_i + \sigma_j\right), \tag{15}$$

$$\varepsilon_{ij} = \left(\varepsilon_i \varepsilon_j\right)^{\frac{1}{2}}. \tag{16}$$

Heat capacity is the ratio of heat absorbed by a material to the temperature change. At sufficiently high temperatures, the heat capacity per atom tends to be the same for all elements. For metals of higher atomic weight, this approximation is already a good one at room temperature, giving rise to the law of Dulong and Petit. For other materials, heat capacity and its temperature variation depend on differences in energy levels for atoms.

The molar heat capacity at constant volume is defined for graphene, graphane, and fluorographene as the partial derivative of the total energy with respect to the temperature:

$$c_v = \left(\frac{\partial E}{\partial T}\right)_v, \tag{17}$$

wherein c_v is the molar heat capacity at constant volume, E is the total energy, T is the temperature, and the subscript v denotes the volume variable held fixed during differentiation.

The empirical law of Dulong and Petit can be represented mathematically as

$$c \cdot M = k, \tag{18}$$

$$k = 3R, \tag{19}$$

in which c is the specific heat capacity, M is the molar mass, k is a constant, and R is the ideal gas constant. The empirical law of Dulong and Petit can be applied only at intermediately high temperatures as an approximation.

For the second-generation reactive empirical bond order potential, the disadvantages arise when modelling a process that involves energetic atomic collisions and ignoring a separate π bond contribution that can understandably cause problems with the overbinding of radicals. In this context, the reactive force-field interatomic potential [39] is utilised for fluorographene to calculate the system energy of the material, which is a powerful computational tool for use in exploration and optimisation of material properties [40]. The reactive force-field method can bridge the gap in simulation scale separating classical and quantum mechanics [39]. In addition, this method describes chemical bonding implicitly by employing a bond-order formalism within a classical approach without expensive quantum mechanics calculations [40]. Unfortunately, the reactive force-field method is subject to certain limitations. For example, it is computationally demanding, and the disadvantage arises from costly algorithms, especially charge equilibration. For the problem involved, other potential functions may be effective and accurate results can be obtained. However, the reactive force-field method offers unique advantages, for example, for describing the dynamics of chemical reactions at an atomistic scale [40], thereby making possible the subsequent research on chemistry. In suspended graphene, a two-dimensional, flexible membrane can exist [33] and ripples spontaneously appear due to strong thermal fluctuations [34]. This means that graphene tends to spontaneous bending and ripple formation.

The system energy of the material can be divided by the reactive force-field method up into various partial energy contributions

$$\begin{aligned} E_{system} = {} & E_{bond} + E_{under\text{-}coordination} + E_{over\text{-}coordination} + E_{valence} \\ & + E_{penalty} + E_{torsion} + E_{conjugation} + E_{van\ der\ Waals} + E_{Coulomb} \end{aligned}, \tag{20}$$

wherein E_{system} is the system energy, E_{bond} is the bond energy, $E_{under\text{-}coordination}$ is the under-coordination energy, $E_{over\text{-}coordination}$ is the over-coordination energy, $E_{valence}$ is the valence angle energy, $E_{penalty}$ is the penalty energy, $E_{torsion}$ is the torsion energy, $E_{conjugation}$ is the conjugation energy, $E_{van\ der\ Waals}$ is the van der Waals energy, and $E_{Coulomb}$ is the Coulomb energy.

The properties of a solid can usually be predicted from the valence and bonding preferences of its constituent atoms. There are many examples of solids that have a single bonding type.

The bond energy can be calculated from the bond order

$$E_{bond} = -D_e \cdot BO_{ij} \cdot e^{p\left(1-BO_{ij}^{p}\right)}, \tag{21}$$

in which D_e is the bond-dissociation enthalpy, also referred to as the bond strength, BO_{ij} is the bond order between a pair of i and j atoms, and p is a bond parameter. Enthalpy is the sum of the internal energy and the product of the pressure and volume of a thermodynamic system. Enthalpy is an energy-like property or state function. As with other energy functions, it is neither convenient nor necessary to determine absolute values of enthalpy. For each substance, the zero-enthalpy state can be some convenient reference state.

With the use of the harmonic approximation, the Fourier transform of the height-height correlation function of a wave vector yields the following equation

$$H\left(q\right) = <|h\left(q\right)|^2> = \frac{Nk_BT}{\kappa S_0 q^4}, \tag{22}$$

wherein H is the height-height correlation function, h is the out-of-plane atomic displacement, N denotes the number of atoms, k_B is the Boltzmann constant, κ is the bending rigidity, S_0 is the area per atom, and q is the wave vector. The Boltzmann constant is a fundamental constant of physics occurring in nearly every statistical formulation of both classical and quantum physics. The physical significance of the Boltzmann constant is that it provides a measure of the amount of energy corresponding to the random thermal motions of the particles making up a substance.

Bending rigidity, or flexural rigidity, is defined as the resistance offered by a structure while undergoing bending. The bending rigidity of the two-dimensional material is determined by the elastic thickness, Poisson's ratio, and Young's modulus. In classical mechanics, the bending rigidity can be derived for an isotropic plate as follows:

$$\kappa\left(h'\right) = \frac{Yh'^3}{12\left(1-\sigma\right)}, \tag{23}$$

where h' is the elastic thickness, Y is the Young's modulus, and σ is the Poisson's ratio. The bending rigidity of a nanomaterial is typically given in electron volts. Young's modulus describes the elastic properties of a solid undergoing tension or compression in only one direction, as in the case of a metal rod that after being stretched or compressed lengthwise returns to its original length. Sometimes referred to as the modulus of elasticity, Young's modulus is equal to the longitudinal stress divided by the strain. The longitudinal strain is called Poisson's ratio.

Anharmonic couplings between stretching and bending modes are of vital importance in the large-wavelength limit

$$H\left(q\right) = \frac{Nk_BT}{\kappa S_0 q^{4-\eta}}, \tag{24}$$

in which η is a scaling exponent, about 0.85 [41, 42]. At finite temperatures, thermally excited intrinsic ripples may cause strong anharmonic effects.

3. Results and discussion

3.1. Relative energy

Different conformations of graphane and fluorographene may differ in stability or energy. Conformation is any one of the infinite numbers of possible spatial arrangements of atoms in a molecule that result from rotation of its constituent groups of atoms about single bonds. Different

conformations are possible for any molecule in which a single covalent bond connects two polyatomic groups, in each of which at least one atom does not lie along the axis of the single bond in question. In general, every distinguishable conformation of a molecule represents a state of different potential energy because of the operation of attractive or repulsive forces that vary with the distances between different parts of the structure. If these forces are absent, all conformations will have the same energy, and rotation about the single bond will be completely free or unrestricted. If the forces are strong, different conformations differ greatly in energy or stability. The molecule will ordinarily occupy a stable state and undergo a transition to another stable state only upon absorbing enough energy to reach and pass through the unstable intervening conformation.

The structures of the graphane and fluorographene isomers are illustrated schematically in Figure 1 with the chair, stirrup, and boat configurations depicted. Grey spheres represent carbon atoms and white spheres represent hydrogen or fluorine atoms. Red and blue spheres represent carbon atoms where hydrogen or fluorine atoms are adsorbed above and below the graphene sheet, respectively. The structural configurations are determined by performing first-principles calculations. Distinguishable conformations exist, and the chair configuration is the most stable structure due to its lowest formation energy. In the present study, molecular dynamics simulations are performed to investigate the thermal properties of the two-dimensional materials and especially the phenomena involved, and their molecules are existed in a chair conformation, in which all the carbon-hydrogen or carbon-fluorine bonds are disposed in a staggered arrangement, as illustrated schematically in Figure 1 with the chair configuration depicted. The carbon atoms of graphene, graphane, or fluorographene are arranged in a flat, planar structure that is a single atom thick. The hydrogen or fluorine atoms are alternately adsorbed above and below the graphene sheet.

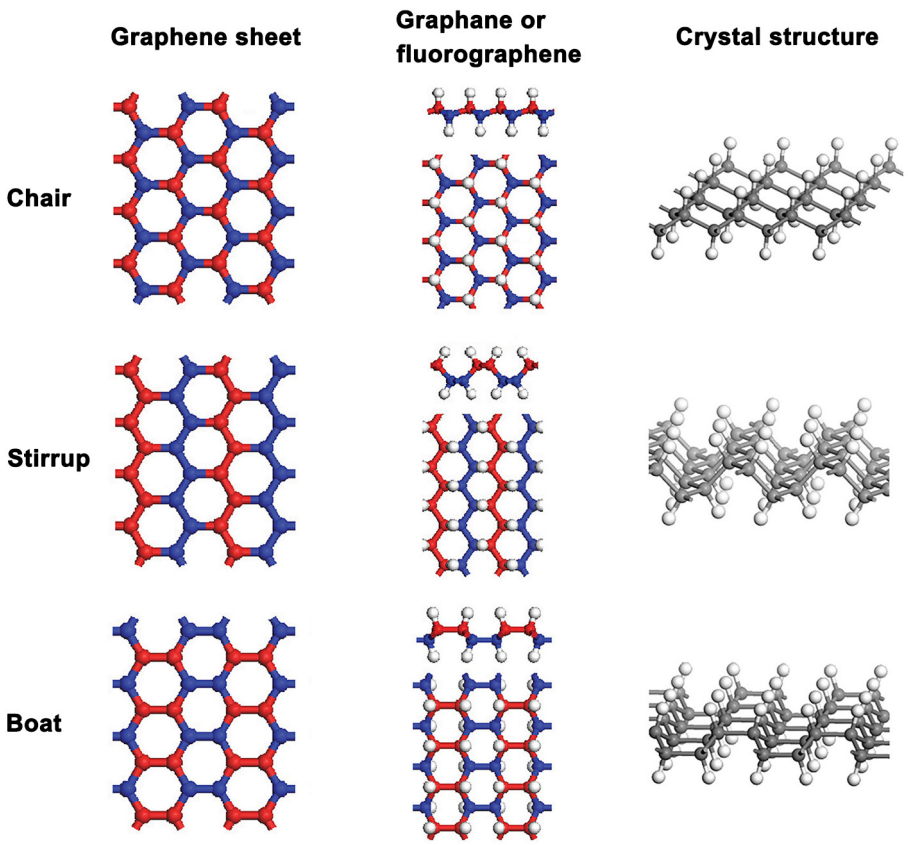

Figure 1. Schematic representation of the structures of the graphane and fluorographene isomers with the chair, stirrup, and boat configurations depicted. Grey spheres represent carbon atoms and white spheres represent hydrogen or fluorine atoms. Red and blue spheres represent carbon atoms where hydrogen or fluorine atoms are adsorbed above and below the graphene sheet, respectively.

The reactive force-field interatomic potential is parametrized against density functional theory calculations. The density-functional theory makes it possible to apply the complicated mathematics of quantum mechanics to the description and analysis of the chemical bonding between atoms. The density-functional theory greatly simplifies the computations needed to understand the electron bonding between atoms within molecules. One example will suffice to illustrate a situation of parameterization for the system containing carbon and fluorine. The properties of the system are determined by applying density functional theory within the Vienna Ab-initio Simulation Package software package [43]. The electron wave functions are calculated using projected augmented wave pseudopotentials and the generalized gradient approximation method [44]. A Monkhorst-Pack k-point mesh of 24 × 24 × 1 is employed for the electronic structure, and an energy cutoff of 600 eV are used. The properties of the system are calculated with Gaussian 16. Molecular relaxed geometries and bond stretching and bending curves are determined at the B3LYP/6-31G* level [45], while atomization and dissociation energies are calculated with the G3 approach [46]. Nonzero point-corrected energies are used. While the change in energy due to bond stretching and bending is calculated at the B3LYP level, curves are shifted in energy to have minima that correspond to G3 values. Various parameters and quantities are determined, for example, the charges of carbon and fluorine atoms in $CH_3-CF_2-CH_3$, the length of the fluorine-fluorine bond in a fluorine molecule, the lengths of the carbon-carbon and carbon-fluorine bonds in $CH_3-CF_2-CH_3$ and $CH_3-CF(CH_3)-CH_3$, the potential energy curve for the dissociation of the carbon-fluorine bond in $CH_3-CF_2-CH_3$, the potential energy curves for the bending the fluorine-carbon-fluorine and carbon-carbon-fluorine bonds in $CH_3-CF_2-CH_3$, and the potential energy curve for the twisting of the fluorine-carbon-carbon-fluorine bond in $CF_2=CF_2$. Various reactions involving fluoroalkanes and fluoroalkenes should be accounted for. Alkenes are compounds made up of hydrogen and carbon that contains one or more pairs of carbon atoms linked by a double bond. Alkenes are examples of unsaturated hydrocarbons.

The relative energy is calculated by applying density functional theory and by using the reactive force-field method, and the results obtained for processes of dissociation of the carbon-fluorine bond in $CH_3-CF_2-CH_3$ and bending of the fluorine-carbon-fluorine bond in $CH_3-CF_2-CH_3$ are presented in Figure 2 for fluorographene with various energy curves defined above. Good agreement is achieved between the results predicted by the reactive force-field method and those calculated by applying density functional theory, such as geometry and energy. Additionally, the carbon-fluorine bond dissociation energy is entirely consistent with that determined by performing quantum mechanical calculations [47]. In most cases, the results are in reasonable agreement with those available in the literature [48]. Consequently, the reactive force-field method is employed in the present study for fluorographene to investigate the thermal properties and especially the phenomena involved. Chemical bonding is any of the interactions that account for the association of atoms into molecules, ions, crystals, and other stable species. If the total energy of a group of atoms is lower than the sum of the energies of the component atoms, they then bond together and the energy lowering is the bonding energy. The energy change accompanying the attachment of electrons to a neutral atom is expressed as the electron affinity, which is the energy released when an electron is attached to an atom of the element. In many cases, the electron affinity is positive, signifying that energy is indeed released when an electron attaches to an atom.

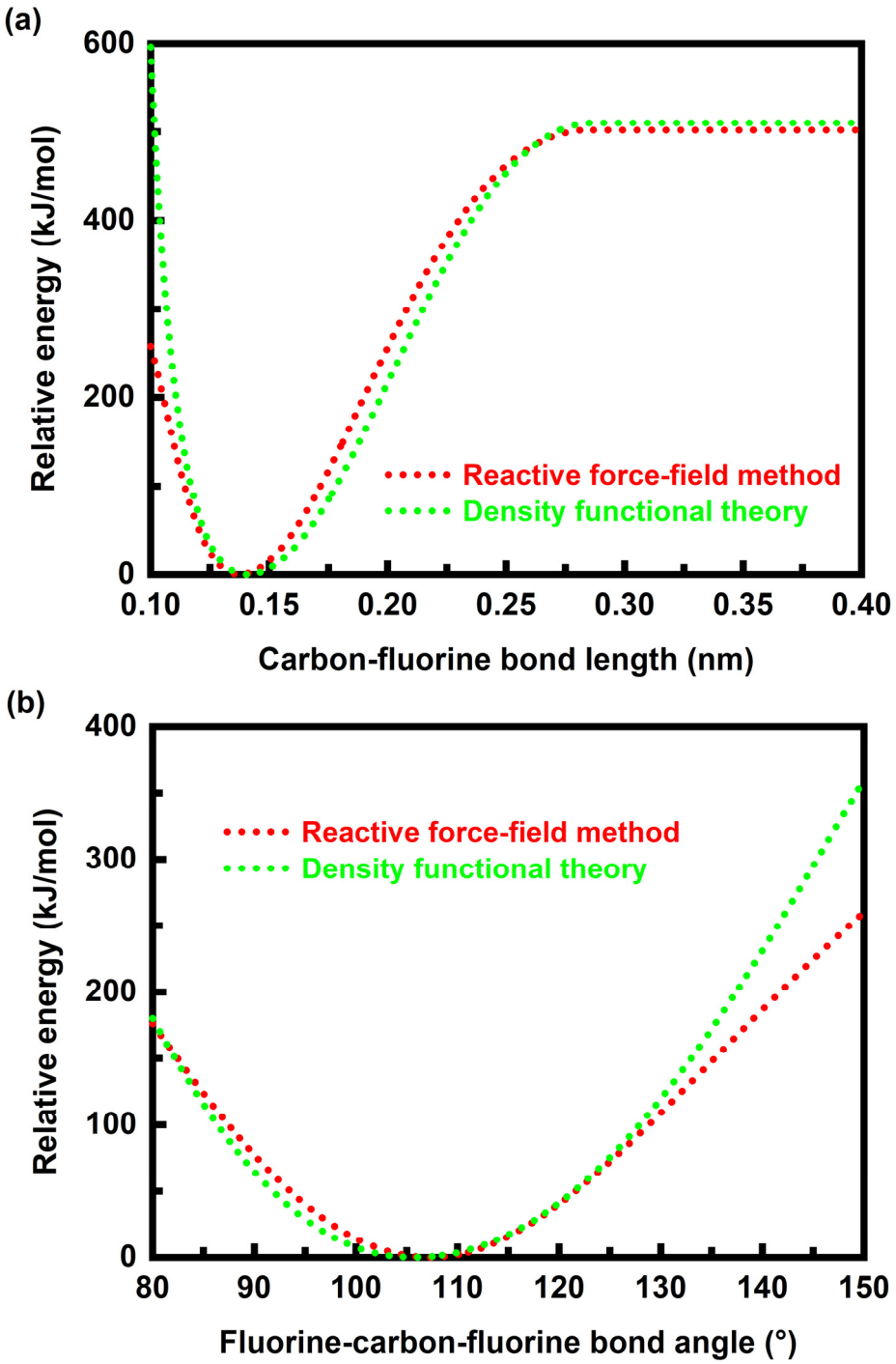

Figure 2. Relative energy as a function of the length or angle of various bonds in fluorographene for different processes. (a) Dissociation of the carbon-fluorine bond in $CH_3-CF_2-CH_3$. (b) Bending of the fluorine-carbon-fluorine bond in $CH_3-CF_2-CH_3$. Comparisons of the relative energy are made between density functional theory and the reactive force-field method.

The results obtained for the relative energy as a function of the length or angle of various bonds in fluorographene are presented in Figure 3 for bending of the carbon-carbon-fluorine bond in $CH_3-CF(CH_3)-CH_3$ and twisting of the fluorine-carbon-carbon-fluorine bond in $CF_2=CF_2$. Good agreement is achieved between the results predicted by the reactive force-field method and those calculated by applying density functional theory, such as geometry and energy. The carbon atoms form a hexagonal or honeycomb lattice, with the nearest neighbour distance 0.1420 nanometres, 0.1536

nanometres, and 0.1579 nanometres, respectively, for graphene, graphane, and fluorographene; The length of the carbon-hydrogen bond in graphane is 0.1104 nanometres; The length of the carbon-fluorine bond in fluorographene is 0.1371 nanometres; The bond angle in graphene is 120°; The angle of the carbon-carbon-carbon bond in graphane and fluorographene is 111.5° and 110.8°, respectively; The angle of the carbon-carbon-hydrogen bond in graphane is 107.4°; The angles of the carbon-carbon-fluorine and fluorine-carbon-fluorine bonds in fluorographene is 108.1° and 107.5°, respectively. The bond length and angle are averaged over the structure of the material.

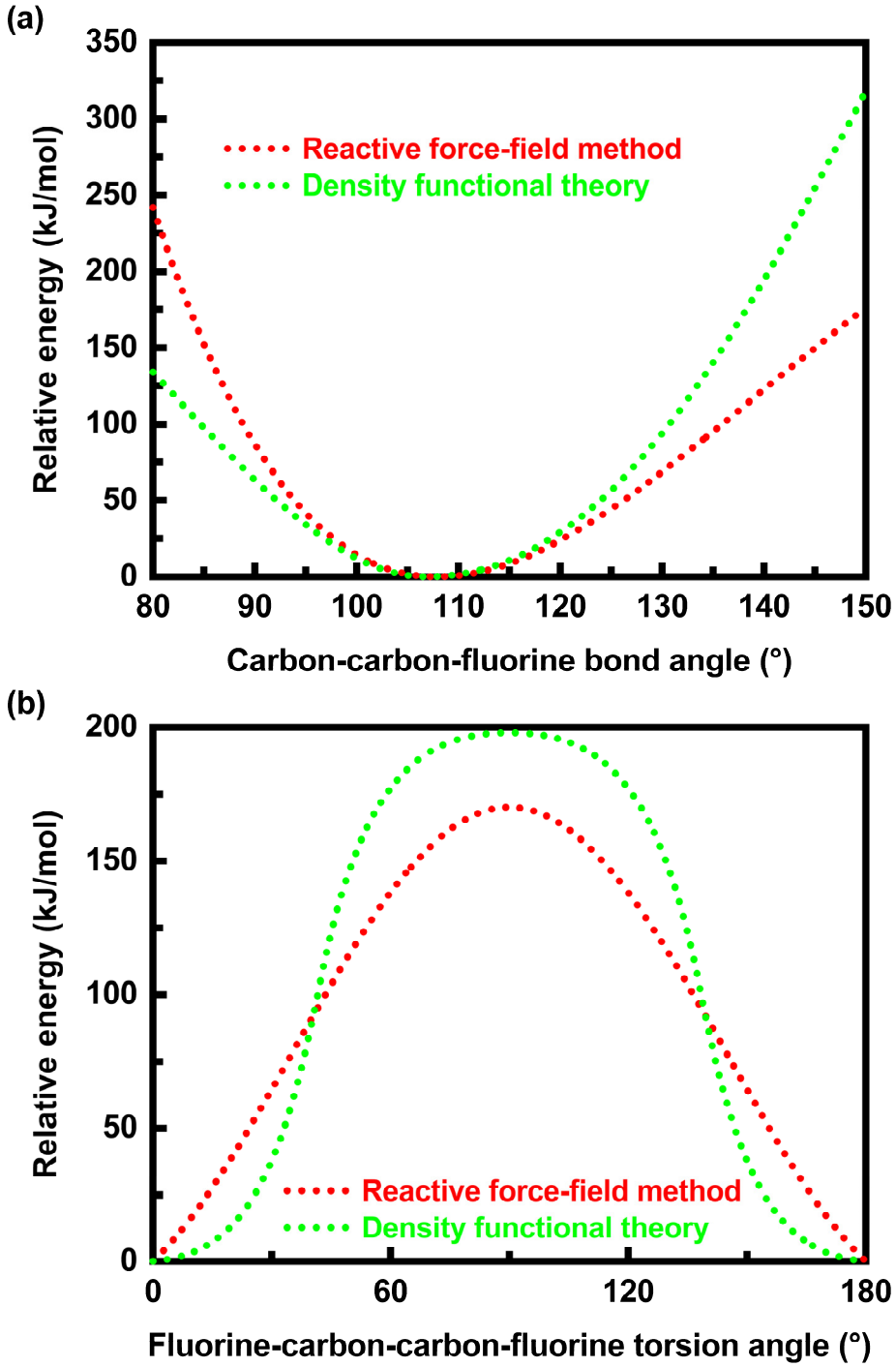

Figure 3. Relative energy as a function of the length or angle of various bonds in fluorographene for different processes. (a) Bending of the carbon-carbon-fluorine bond in $CH_3\text{-}CF(CH_3)\text{-}CH_3$. (b) Twisting of the fluorine-carbon-carbon-fluorine bond in $CF_2=CF_2$. Comparisons of the relative energy are made between density functional theory and the reactive force-field method.

3.2. Thermal contraction

The effect of temperature on the thermal expansion coefficient of graphene, graphane, and fluorographene is illustrated in Figure 4 in which both graphene and graphane have a thermal contraction property. The shaded region demarcates the regime of thermal contraction, in which there is a general decrease in the volume of the isometric material as the temperature is raised. More generally, graphene and graphane contract or expand when subjected to changes in temperature. Fluorographene does not contract as the temperature is raised, namely it has not a thermal contraction property. In such a context, comparisons are made only between graphene and graphane in terms of thermal contraction. In most cases, the two-dimensional materials contract as their temperature rises. For example, at room temperature, the thermal expansion coefficient is about -9.69×10^{-5}/K for graphene, about -2.88×10^{-4}/K for graphane, and about 5.77×10^{-5}/K for fluorographene, respectively. Both graphene and graphane have negative thermal expansion properties over an extended temperature range, specifically, at temperatures below about 1150 K. However, graphane is thermally contracted more significantly than graphene. Contraction with increasing temperature or negative thermal expansion is a potentially useful and unusual property for a crystalline material [49, 50], and very few solid materials possess strongly negative expansions over a broad temperature range [51, 52]. For both graphene and graphane, the coefficient of thermal expansion increases as their temperature is increased. However, differences do exist, as the two materials have different thermal expansion coefficients. Specifically, at lower temperatures, the thermal expansion coefficient of graphane is much lower than that of graphene. This may be caused by intrinsic ripples due to the effect of random thermal fluctuations of hydrogen atoms. In the crystals, there is a dynamic balance between the conditions created by temperature and the cohesive forces holding the atoms together. The two materials have different bonding forces, thus enabling different thermal expansion coefficients.

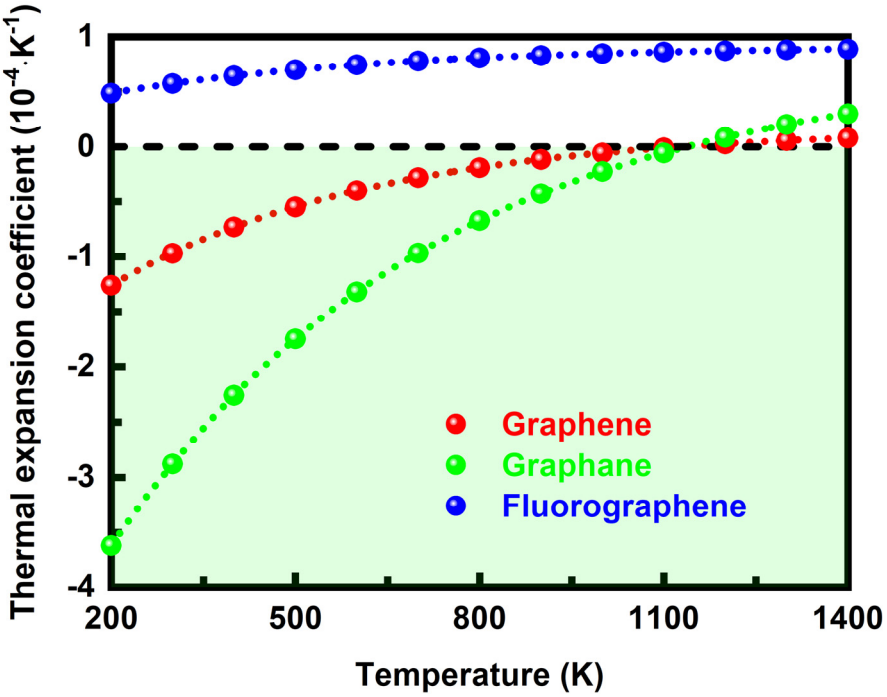

Figure 4. Thermal expansion coefficients of graphene, graphane, and fluorographene at different temperatures. The shaded region demarcates the regime of thermal contraction.

The change in volume per unit temperature change becomes insignificant at higher temperatures, as illustrated in Figure 4 by the thermal expansion coefficients. As the temperature is raised, a change in the thermal expansion coefficient beyond a threshold, namely zero in this situation, serves as an indication that the isometric material is no longer is thermally contracted. Thermal expansion does occur at higher temperatures, and the two-dimensional materials expand slightly as their temperature is

increased. Specifically, at temperatures in excess of 1200 K, both graphene and graphane have about zero or positive coefficients of thermal expansion. Consequently, the two-dimensional materials contract at low and moderate temperatures and expand slightly at high temperatures, when they are heated. Graphene and graphane have negative coefficients of thermal expansion, which is particularly useful for specific applications. Elastomer properties can be tailored to specific applications. For example, the control of thermal expansion is of particularly importance [53]. Elastomers usually have notoriously high expansion coefficients, therefore limiting their use in a variety of practical technology applications [54]. Graphane has significantly negative coefficients of thermal expansion, and therefore it can be incorporated into an elastomer to form a composite material with negative, zero, or reduced net coefficients of thermal expansion. The temperature considered here varies from 200 K to 1400 K, which does not exceed the stability limit of each material. Excessively high temperatures can cause loss of physicochemical stability of the materials. Additionally, at very high temperatures, a phase change may occur and the effect of thermal radiation becomes significant. In such a situation, fluid mechanics, especially computational fluid dynamics, is effective in understanding the causes of the thermal phenomena involved. Further study is needed to calculate the thermal expansion coefficients of partially hydrogenated or fluorinated graphene, thereby elucidating the effect of hydrogenation or fluorination degree. Unfortunately, the study is computationally demanding. Additionally, there is still confusion as to whether or not partially hydrogenated or fluorinated graphene contracts when subjected to changes in temperature, as the problem is very complicated.

3.3. Heat capacity

The heat capacity of a two-dimensional material, defined as ratio of heat absorbed to the temperature change, determines not only how quickly the material heats but also the thermal energy stored within the material [55, 56]. In the present study, the solution to the heat capacity problem can be reached by conducting numerical analysis on the energy data obtained, namely by numerically calculating the partial derivative of the total energy with respect to the temperature. Heat capacities are calculated at different temperatures for both graphane and fluorographene using the method descried in detail above and the formulation of the empirical law of Dulong and Petit. The formulation is used only as an approximation and valid only for intermediately high temperatures.

The effect of temperature on the potential energy per atom is illustrated in Figure 5 for graphene, graphane, and fluorographene. The negative potential energy is related closely to the positive binding energy. Binding energy is the amount of energy required to separate a crystal completely into its constituent atoms. Graphane has a binding energy per carbon atom greater than graphene. A negative relationship does exist between the binding energy and the temperature. More specifically, the binding energy decreases as the temperature is raised. The binding energy for graphene varies from about 7.42 eV per atom to about 7.63 eV per atom. In contrast, the binding energy of carbon atoms in graphane varies from about 7.69 eV per atom to about 8.08 eV per atom. However, the effect of temperature on the binding energy of hydrogen atoms in graphane becomes less pronounced. At a temperature of 50 K, graphane has an approximate binding energy of 5.22 eV per atom, which is comparable to the binding energy, 5.19 eV per atom, obtained from the density functional theory calculations. Graphene has an approximate binding energy of 7.63 eV per atom at a temperature of 50 K. Additionally, the binding energy of a single carbon atom in graphene decreases slightly with temperature. The binding energy of carbon atoms in fluorographene varies from about 7.02 eV per atom to about 7.32 eV per atom. Therefore, fluorographene has a binding energy per carbon atom less than graphene and graphane. However, the binding energy of fluorine atoms in fluorographene is very high and the effect of temperature becomes more pronounced. Accordingly, fluorographene has a binding energy per atom greater than graphene and graphane, especially at lower temperatures. For example, at a temperature of 50 K, fluorographene has an approximate binding energy of 8.64 eV per atom.

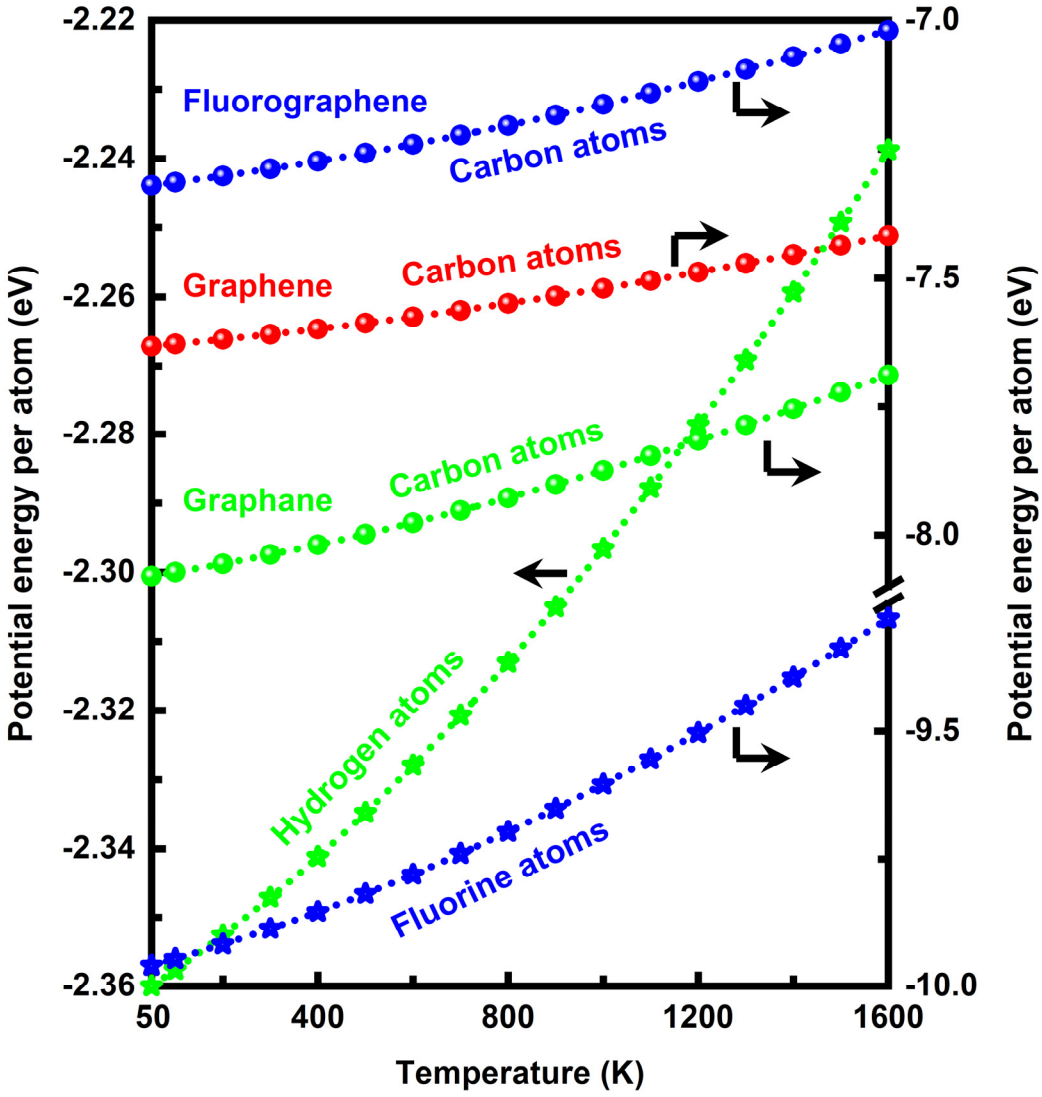

Figure 5. Effect of temperature on the potential energy of graphene, graphane, and fluorographene per atom. The negative potential energy is related closely to the positive binding energy. A right-Y scale is added to the graph and the carbon and fluorine atoms' data are plotted against this scale, as indicated by the rightwards arrows.

The effect of temperature on the total energy per carbon atom is illustrated in Figure 6 for graphene, graphane, and fluorographene. The total energy of a group of atoms for graphane is calculated as the sum of the kinetic and potential energy of carbon and hydrogen atoms bound together in the crystal. A similar approach is applied to fluorographene. A positive relationship does exist between the total energy and the temperature. Additionally, the total energy increases with increasing the temperature. The heat capacities are calculated from the energy data presented in Figures 5 and 6, and numerical analysis is needed to solve the problem. In the temperature range from 500 K to 1600 K, the calculated average molar heat capacity at constant volume is about 25.00 J/(mol·K) for graphene, about 29.26 J/(mol·K) for graphane, and about 35.78 J/(mol·K) for fluorographene, respectively. The molar heat capacity of graphene at constant volume is substantially consistent with that calculated by applying the empirical law of Dulong and Petit, which is about 24.94 J/(mol·K). The molar heat capacity of graphene is also in good agreement with that calculated using the Monte Carlo method based upon the LCBOPII empirical potential. A higher molar heat capacity is obtained for graphane because extra vibrational energy is stored in the carbon-hydrogen bonds. Specifically, graphane has a molar heat capacity of 17 percent higher than graphene. Similarly, fluorographene has a molar heat capacity of 43 percent higher than graphene due to extra vibrational energy stored.

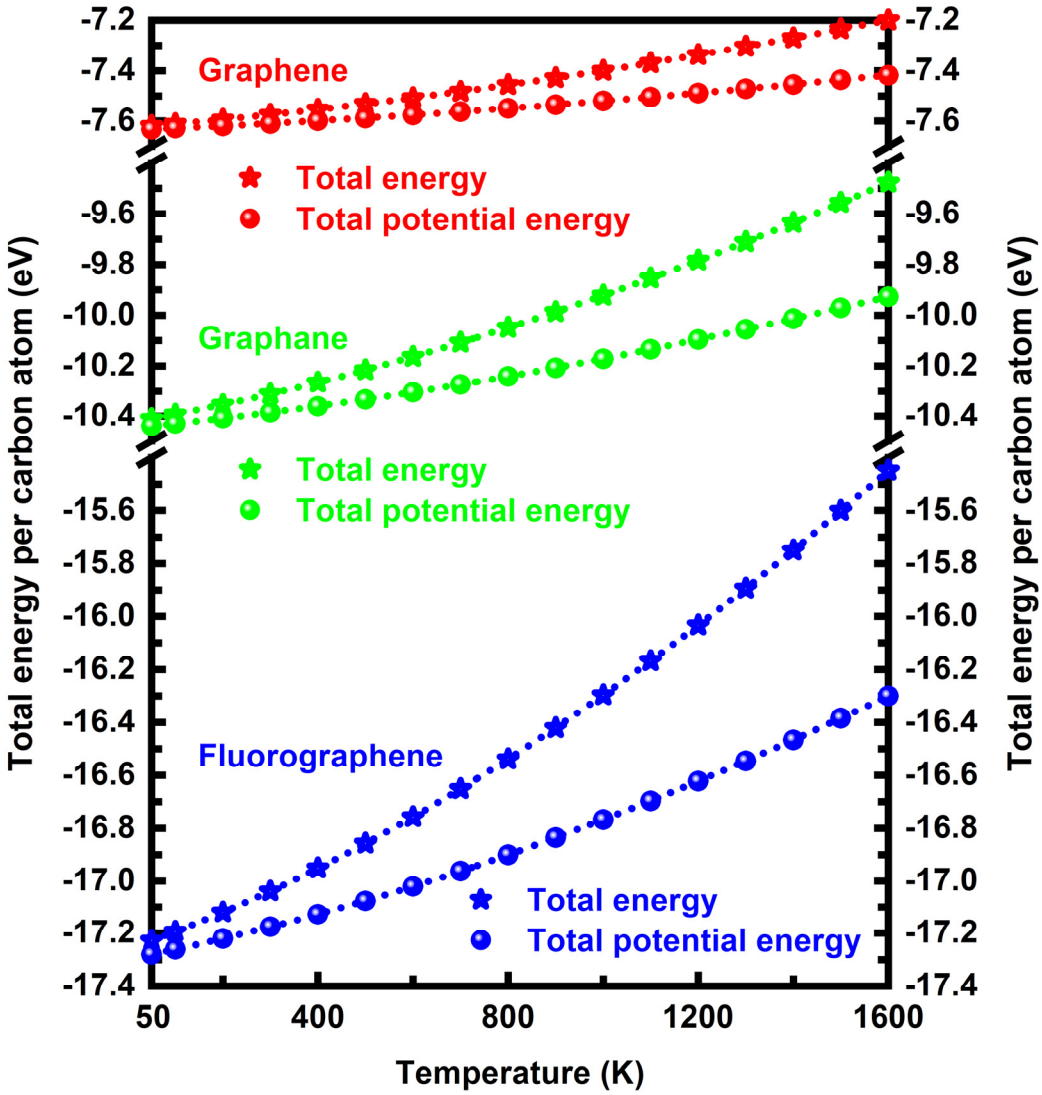

Figure 6. Effect of temperature on the total energy of graphene, graphane, and fluorographene per carbon atom. The total energy is calculated as the sum of the kinetic and potential energy.

The heat capacity at constant volume is calculated using the phonon dispersion relations with the density of states [57, 58]. There are significant differences in phonon spectra between graphane and fluorographene, and therefore their thermal properties may be sufficiently different from each other [57, 58]. The effect of temperature on the molar heat capacity at constant volume is illustrated in Figure 7 for graphene, graphane, and fluorographene, wherein the heat capacity is calculated with two different approaches, namely using the phonon dispersion relations and by carrying out numerical analysis on the total energy data obtained. The effect of temperature on the specific heat capacity at constant volume is illustrated in Figure 8 for comparison purposes. Reasonable agreements on heat capacity are reached between the two approaches. Consequently, the numerical approach provides an alternative way to determine the heat capacities of the two-dimensional materials. At room temperature, the molar heat capacity at constant volume that is calculated using the phonon dispersion relations is about 8.16 J/(mol·K) for graphene, about 12.41 J/(mol·K) for graphane, and about 20.70 J/(mol·K) for fluorographene, respectively. The heat capacities of the two-dimensional materials tend to become zero at sufficiently low temperatures. Additionally, the molar heat capacity at constant volume differs from each other at sufficiently high temperatures. In general, the molar heat capacity of fluorographene is higher than that of graphane. In contrast, the specific heat capacity of fluorographene is lower than that of graphane due to the difference in molecular weight between the two two-dimensional materials. Fluorographene is more than twice the molecular weight of graphane. The difference in the heat

capacity at constant volume becomes remarkable at higher temperatures. For example, at a temperature of 1000 K, graphane is about twice the specific heat capacity of fluorographene, as determined approximatively on the basis of the empirical law of Dulong and Petit. Significant differences in phonon spectra manifest themselves in the heat capacity graphane and fluorographene have. Graphene has lower molar heat capacities in the temperature range. In most cases, however, its specific heat capacities are still higher than those of fluorographene.

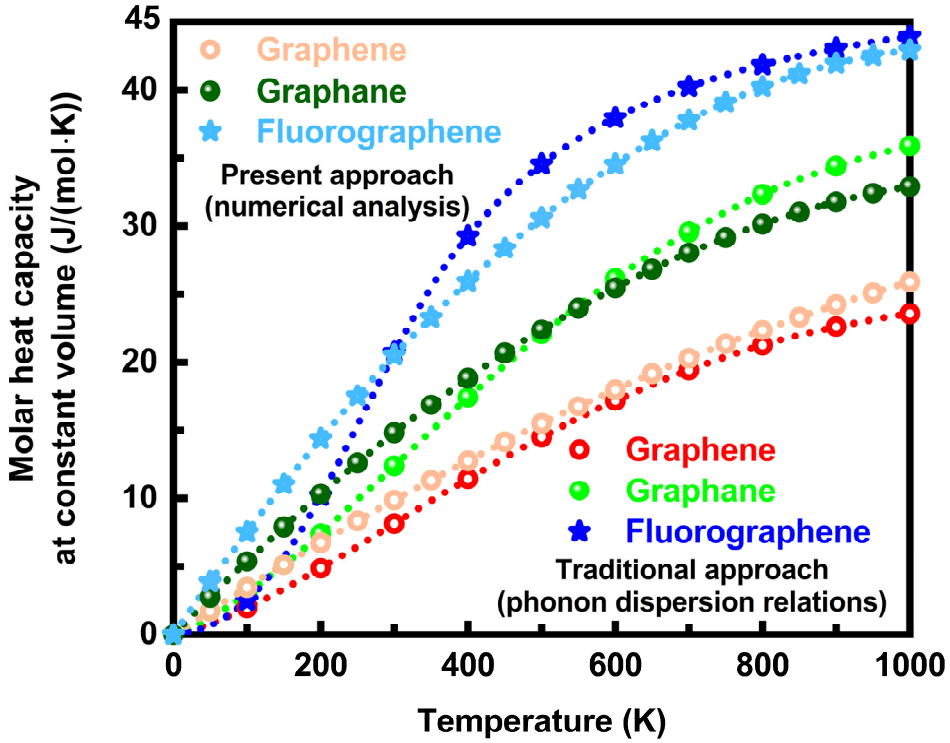

Figure 7. Effect of temperature on the molar heat capacity of graphene, graphane, and fluorographene at constant volume. The heat capacity is calculated using the phonon dispersion relations and by carrying out numerical analysis on the total energy data obtained.

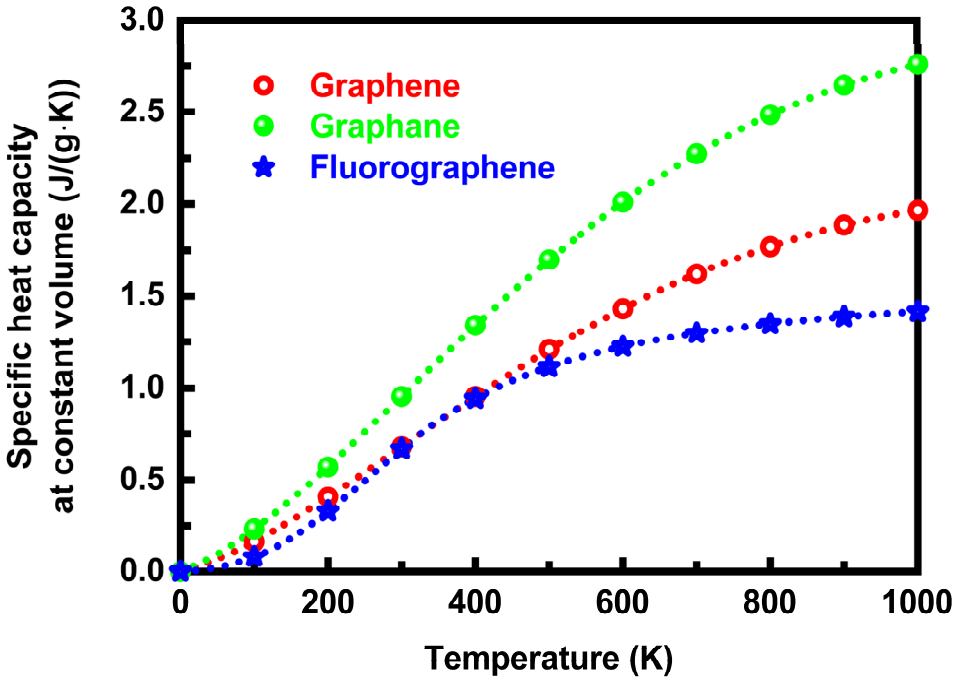

Figure 8. Effect of temperature on the specific heat capacity of graphene, graphane, and fluorographene at constant volume. Specific heat capacity is the quantity of heat required to raise the temperature per unit mass.

4. Conclusions

Molecular dynamics was used to investigate the thermal properties of graphane and fluorographene and especially the phenomena involved in the thermodynamic process when subjected to changes in temperature, including thermal expansion coefficients and heat capacities, which have profound implications for the development of thermal technology at the nanoscale. Additionally, first-principles calculations were carried out to determine the structural configurations of the two-dimensional materials. Furthermore, comparisons of thermal properties and the phenomena involved were made between pristine and functionalised graphene. The main conclusions are summarised as follows:

- Both graphene and graphane have negative thermal expansion properties at temperatures below about 1150 K, but graphane is thermally contracted more significantly than graphene. Fluorographene does not contract as the temperature is raised.
- A negative relationship does exist between the binding energy and the temperature.
- The heat capacity results are validated by different calculation methods.
- Fluorographene has a molar heat capacity higher than graphane and a specific heat capacity lower than graphane.
- At room temperature, the thermal expansion coefficient is about -2.88×10^{-4}/K for graphane and about 5.77×10^{-5}/K for fluorographene, and the molar heat capacity at constant volume is about 12.41 J/(mol·K) for graphane and about 20.70 J/(mol·K) for fluorographene.
- In the temperature range from 500 K to 1600 K, the calculated average molar heat capacity at constant volume is about 29.26 J/(mol·K) for graphane and about 35.78 J/(mol·K) for fluorographene.

References

[1] Bolotin, K. I.; Ghahari, F.; Shulman, M. D.; Stormer, H. L.; Kim, P. Observation of the fractional quantum Hall effect in graphene. *Nature* **2009**, *462* (7270), 196-199.

[2] Dean, C. R.; Young, A. F.; Cadden-Zimansky, P.; Wang, L.; Ren, H.; Watanabe, K.; Taniguchi, T.; Kim, P.; Hone, J.; Shepard, K. L. Multicomponent fractional quantum Hall effect in graphene. *Nature Phys.* **2011**, *7* (9), 693-696.

[3] Baringhaus, J.; Ruan, M.; Edler, F.; Tejeda, A.; Sicot, M.; Taleb-Ibrahimi, A.; Li, A. -P.; Jiang, Z.; Conrad, E. H.; Berger, C.; Tegenkamp, C.; de Heer, W. A. Exceptional ballistic transport in epitaxial graphene nanoribbons. *Nature* **2014**, *506* (7488), 349-354.

[4] Novoselov, K. S.; Geim, A. K.; Morozov, S. V.; Jiang, D.; Zhang, Y.; Dubonos, S. V.; Grigorieva, I. V.; Firsov, A. A. Electric field effect in atomically thin carbon films. *Science* **2004**, *306* (5696), 666-669.

[5] Mao, S.; Wang, Z.; Luo, Q.; Lu, B.; Wang, Y. Geometric and electronic effects in hydrogenation reactions. *ACS Catal.* **2023**, *13* (2), 974-1019.

[6] Ren, Y.; Yang, Y.; Wei, M. Recent advances on heterogeneous non-noble metal catalysts toward selective hydrogenation reactions. *ACS Catal.* **2023**, *13* (13), 8902-8924.

[7] Boukhvalov, D. W.; Katsnelson, M. I.; Lichtenstein, A. I. Hydrogen on graphene: Electronic structure, total energy, structural distortions and magnetism from first-principles calculations. *Phys. Rev. B* **2008**, *77* (3), 035427.

[8] Sofo, J. O.; Chaudhari, A. S.; Barber, G. D. Graphane: A two-dimensional hydrocarbon. *Phys. Rev. B* **2007**, *75* (15), 153401.

[9] Gao, H.; Wang, L.; Zhao, J.; Ding, F.; Lu, J. Band gap tuning of hydrogenated graphene: H

coverage and configuration dependence. *J. Phys. Chem. C* **2011**, *115* (8), 3236-3242.
[10] Jaiswal, M.; Lim, C. H. Y. X.; Bao, Q.; Toh, C. T.; Loh, K. P.; Özyilmaz, B. Controlled hydrogenation of graphene sheets and nanoribbons. *ACS Catal.* **2011**, *5* (2), 888-896.
[11] Grassi, R.; Low, T.; Lundstrom, M. Scaling of the energy gap in pattern-hydrogenated graphene. *Nano Lett.* **2011**, *11* (11), 4574-4578.
[12] Friedman, A. L.; van't Erve, O. M. J.; Robinson, J. T.; Whitener, Jr., K. E.; Jonker, B. T. Hydrogenated graphene as a homoepitaxial tunnel barrier for spin and charge transport in graphene. *ACS Nano* **2015**, *9* (7), 6747-6755.
[13] Buonocore, F.; Capasso, A.; Celino, M.; Lisi, N.; Pulci, O. Tuning the electronic properties of graphane via hydroxylation: An ab initio study. *J. Phys. Chem. C* **2021**, *125* (29), 16316-16323.
[14] Li, Y.; Zhou, Z.; Shen, P.; Chen, Z. Structural and electronic properties of graphane nanoribbons. *J. Phys. Chem. C* **2009**, *113* (33), 15043-15045.
[15] Son, J.; Lee, S.; Kim, S. J.; Park, B. C.; Lee, H. -K.; Kim, S.; Kim, J. H.; Hong, B. H.; Hong, J. Hydrogenated monolayer graphene with reversible and tunable wide band gap and its field-effect transistor. *Nat. Commun.* **2016**, *7*, 13261.
[16] Jiang, L.; Fu, W.; Birdja, Y. Y.; Koper, M. T. M.; Schneider, G. F. Quantum and electrochemical interplays in hydrogenated graphene. *Nat. Commun.* **2018**, *9*, 793.
[17] Singh, A. K.; Penev, E. S.; Yakobson, B. I. Vacancy clusters in graphane as quantum dots. *ACS Nano* **2010**, *4* (6), 3510-3514.
[18] Zhang, L. Z.; Zhai, F.; Jin, K. -H.; Cui, B.; Huang, B.; Wang, Z.; Lu, J. Q.; Liu, F. Quantum spin hall effect and tunable spin transport in as-graphane. *Nano Lett.* **2017**, *17* (7), 4359-4364.
[19] Elias, D. C.; Nair, R. R.; Mohiuddin, T. M. G.; Morozov, S. V.; Blake, P.; Halsall, M. P.; Ferrari, A. C.; Boukhvalov, D. W.; Katsnelson, M. I.; Geim, A. K.; Novoselov, K. S. Control of graphene's properties by reversible hydrogenation: Evidence for graphane. *Science* **2009**, *323* (5914), 610-613.
[20] Fei, Y.; Fang, S.; Hu, Y. H. Synthesis, properties and potential applications of hydrogenated graphene. *Chem. Eng. J.* **2020**, *397*, 125408.
[21] Padamata, S. K.; Yasinskiy, A.; Stopic, S.; Friedrich, B. Fluorination of two-dimensional graphene: A review. *J. Fluor. Chem.* **2022**, *255-256*, 109964.
[22] Chronopoulos, D. D.; Bakandritsos, A.; Pykal, M.; Zbořil, R.; Otyepka, M. Chemistry, properties, and applications of fluorographene. *Appl. Mater. Today* **2017**, *9*, 60-70.
[23] Chen, X.; Fan, K.; Liu, Y.; Li, Y.; Liu, X.; Feng, W.; Wang, X. Recent advances in fluorinated graphene from synthesis to applications: Critical review on functional chemistry and structure engineering. *Adv. Mater.* **2022**, *34* (1), 2101665.
[24] Nair, R. R.; Ren, W.; Jalil, R.; Riaz, I.; Kravets, V. G.; Britnell, L.; Blake, P.; Schedin, F.; Mayorov, A. S.; Yuan, S.; Katsnelson, M. I.; Cheng, H. -M.; Strupinski, W.; Bulusheva, L. G.; Okotrub, A. V.; Grigorieva, I. V.; Grigorenko, A. N.; Novoselov, K. S.; Geim, A. K. Fluorographene: A two-dimensional counterpart of Teflon. *Small* **2010**, *6* (24), 2877-2884.
[25] Schleder, G. R.; Marinho, Jr., E.; Baquiao, D. J. R.; Celaschi, Y. M.; Gollino, F.; Dalpian, G. M.; Autreto, P. A. S. Tuning hydrogen adsorption and electronic properties from graphene to fluorographone. *Phys. Rev. Materials* **2020**, *4* (7), 074005.
[26] Rajeena, U.; Raveendran, P.; Ramakrishnan, R. M. Stepwise defluorination of fluorographene: How do the structural features govern the rates of heterogeneous electron transfer? *J. Fluor. Chem.* **2020**, *235*, 109555.
[27] Robinson, J. T.; Burgess, J. S.; Junkermeier, C. E.; Badescu, S. C.; Reinecke, T. L.; Perkins, F. K.; Zalalutdniov, M. K.; Baldwin, J. W.; Culbertson, J. C.; Sheehan, P. E.; Snow, E. S. Properties of fluorinated graphene films. *Nano Lett.* **2010**, *10* (8), 3001-3005.

[28] Bourlinos, A. B.; Safarova, K.; Siskova, K.; Zbořil, R. The production of chemically converted graphenes from graphite fluoride. *Carbon* **2012**, *50* (3), 1425-1428.
[29] Javaid, S.; Anjum, M. A. R.; Khan, R. T. A.; Akhtar, M. J. Electronic structure of partially fluorinated graphene: The impact of adsorption patterns and dynamic stability. *Chem. Phys. Lett.* **2022**, *803*, 139807.
[30] Cheng, L.; Jandhyala, S.; Mordi, G.; Lucero, A. T.; Huang, J.; Azcatl, A.; Addou, R.; Wallace, R. M.; Colombo, L.; Kim, J. Partially fluorinated graphene: Structural and electrical characterization. *ACS Appl. Mater. Interfaces* **2016**, *8* (7), 5002-5008.
[31] Pedram, Y.; Marsusi, F.; Yousefbeigi, S. Melting process of fluorinated graphene: A molecular dynamics study. *Chem. Phys. Lett.* **2021**, *780*, 138920.
[32] Lai, W.; Xu, D.; Wang, X.; Wang, Z.; Liu, Y.; Zhang, X.; Liu, X. Characterization of the thermal/thermal oxidative stability of fluorinated graphene with various structures. *Phys. Chem. Chem. Phys.* **2017**, *19* (29), 19442-19451.
[33] Meyer, J. C.; Geim, A. K.; Katsnelson, M. I.; Novoselov, K. S.; Booth, T. J.; Roth, S. The structure of suspended graphene sheets. *Nature* **2007**, *446* (7131), 60-63.
[34] Fasolino, A.; Los, J. H.; Katsnelson, M. I. Intrinsic ripples in graphene. *Nature Mater.* **2007**, *6*, 858-861.
[35] Trędak, P.; Rudnicki, W. R.; Majewski, J. A. Efficient implementation of the many-body Reactive Bond Order (REBO) potential on GPU. *J. Comput. Phys.* **2016**, *321*, 556-570.
[36] Chil, C.; Durinck, J.; Coupeau, C. Buckling of graphene under compressive strain: DFT calculations and second generation REBO potential. *Extreme Mech. Lett.* **2022**, *56*, 101845.
[37] Kemper, T. W.; Sinnott, S. B. Mechanisms of ion-beam modification of terthiophene oligomers from atomistic simulations. *J. Phys. Chem. C* **2011**, *115* (48), 23936-23945.
[38] Choudhary, K.; Hill, L. B.; Glosser, C.; Kemper, T. W.; Bucholz, E. W.; Sinnott, S. B. Atomic-scale quantification of the chemical modification of polystyrene through S, SC, and SH deposition from molecular dynamics simulations. *J. Phys. Chem. C* **2013**, *117* (23), 12103-12110.
[39] van Duin, A. C. T.; Dasgupta, S.; Lorant, F.; Goddard, W. A. ReaxFF: A reactive force field for hydrocarbons. *J. Phys. Chem. A* **2001**, *105* (41), 9396-9409.
[40] Senftle, T. P.; Hong, S.; Islam, M. M.; Kylasa, S. B.; Zheng, Y.; Shin, Y. K.; Junkermeier, C.; Engel-Herbert, R.; Janik, M. J.; Aktulga, H. M.; Verstraelen, T.; Grama, A.; van Duin, A. C. T. The ReaxFF reactive force-field: Development, applications and future directions. *npj Comput. Mater.* **2016**, *2*, 15011.
[41] Kownacki, J. -P.; Mouhanna, D. Crumpling transition and flat phase of polymerized phantom membranes. *Phys. Rev. E* **2009**, *79* (4), 040101(R).
[42] Los, J. H.; Katsnelson, M. I.; Yazyev, O. V.; Zakharchenko, K. V.; Fasolino, A. Scaling properties of flexible membranes from atomistic simulations: Application to graphene. *Phys. Rev. B* **2009**, *80* (12), 121405(R).
[43] Kresse, G.; Hafner, J. *Ab initio* molecular dynamics for liquid metals. *Phys. Rev. B* **1993**, *47* (1), 558-561.
[44] Becke, A. D. Density-functional exchange-energy approximation with correct asymptotic behavior. *Phys. Rev. A* **1988**, *38* (6), 3098-3100.
[45] Becke, A. D. Density-functional thermochemistry. III. The role of exact exchange. *J. Chem. Phys.* **1993**, *98* (7), 5648-5652.
[46] Curtiss, L. A.; Raghavachari, K.; Redfern, P. C.; Rassolov, V.; Pople, J. A. Gaussian-3 (G3) theory for molecules containing first and second-row atoms. *J. Chem. Phys.* **1998**, *109* (18), 7764-7776.
[47] Dubecký, M.; Otyepková, E.; Lazar, P.; Karlický, F.; Petr, M.; Čépe, K.; Banáš, P.; Zbořil, R.; Otyepka, M. Reactivity of fluorographene: A facile way toward graphene derivatives. *J. Phys.*

Chem. Lett. **2015**, *6* (8), 1430-1434.
[48] Paupitz, R.; Autreto, P. A. S.; Legoas, S. B.; Srinivasan, S. G.; van Duin, A. C. T.; Galvão, D. S. Graphene to fluorographene and fluorographane: A theoretical study. *Nanotechnology* **2013**, *24* (3), 035706.
[49] Sleight, A. W. Thermal contraction. *Nature* **1997**, *389* (6654), 923-924.
[50] Zheng, X. G.; Kubozono, H.; Yamada, H.; Kato, K.; Ishiwata, Y.; Xu, C. N. Giant negative thermal expansion in magnetic nanocrystals. *Nat. Nanotechnol.* **2008**, *3*, 724-726.
[51] Kong, Y.; Yin, Y.; Feng, X.; Zhang, Z.; Ding, F.; Tong, L.; Zhang, J. Negative thermal expansion behaviour of graphdiyne. *Nano Today* **2023**, *48*, 101695.
[52] Kriegel, M. A.; Omambac, K. M.; Franzka, S.; zu Heringdorf, F. -J. M.; Hoegen, M. H. Incommensurability and negative thermal expansion of single layer hexagonal boron nitride. *Appl. Surf. Sci.* **2023**, *624*, 157156.
[53] Lunkenheimer, P.; Loidl, A.; Riechers, B.; Zaccone, A.; Samwer, K. Thermal expansion and the glass transition. *Nature Phys.* **2023**, *19*, 694-699.
[54] Kim, B.; Park, M.; Kim, Y. S.; Jeong, U. Thermal expansion and contraction of an elastomer stamp causes position-dependent polymer patterns in capillary force lithography. *ACS Appl. Mater. Interfaces* **2011**, *3* (12), 4695-4702.
[55] Xia, M.; Song, Y.; Zhang, S. Specific heat of graphene nanoribbons. *Phys. Lett. A* **2011**, *375* (42), 3726-3730.
[56] Neek-Amal, M.; Peeters, F. M. Lattice thermal properties of graphane: Thermal contraction, roughness, and heat capacity. *Phys. Rev. B* **2011**, *83* (23), 235437.
[57] Peelaers, H.; Hernández-Nieves, A. D.; Leenaerts, O.; Partoens, B.; Peeters, F. M. Vibrational properties of graphene fluoride and graphane. *Appl. Phys. Lett.* **2011**, *98* (5), 051914.
[58] Ulmet, J. P.; Bachère, L.; Askenazy, S.; Ousset, J. C. Negative magnetoresistance in some dimethyltrimethylene-tetraselenafulvalenium salts: A signature of weak-localization effects. *Phys. Rev. B* **1988**, *38* (11), 7782-7788.